IOP Publishing Bioinspir. Biomim. 20 (2025) 016024 https://doi.org/10.1088/1748-3190/ad9535

Bioinspiration & Biomimetics

PAPER

Stability and agility trade-offs in spring-wing systems

James Lynch[1], Ethan S Wold[2], Jeff Gau[3], Simon Sponberg[2,4] and Nick Gravish[1,*]

[1] Department of Mechanical & Aerospace Engineering, University of California, San Diego, CA, United States of America
[2] School of Biological Sciences, Georgia Institute of Technology, Atlanta, GA, United States of America
[3] Interdisciplinary Bioengineering Graduate Program and George W. Woodruff School of Mechanical Engineering, Georgia Institute of Technology, Atlanta, GA, United States of America
[4] School of Physics, Georgia Institute of Technology, Atlanta, GA, United States of America
[*] Author to whom any correspondence should be addressed.

E-mail: ngravish@ucsd.edu

RECEIVED
17 July 2024

REVISED
2 November 2024

ACCEPTED FOR PUBLICATION
20 November 2024

PUBLISHED
23 December 2024

Keywords: insect flight, resonance, dynamic scaling, elasticity, robophysics

Abstract

Flying insects are thought to achieve energy-efficient flapping flight by storing and releasing elastic energy in their muscles, tendons, and thorax. However, 'spring-wing' flight systems consisting of elastic elements coupled to nonlinear, unsteady aerodynamic forces present possible challenges to generating stable and responsive wing motion. The energetic efficiency from resonance in insect flight is tied to the Weis-Fogh number (N), which is the ratio of peak inertial force to aerodynamic force. In this paper, we present experiments and modeling to study how resonance efficiency (which increases with N) influences the control responsiveness and perturbation resistance of flapping wingbeats. In our first experiments, we provide a step change in the input forcing amplitude to a series-elastic spring-wing system and observe the response time of the wing amplitude increase. In our second experiments we provide an external fluid flow directed at the flapping wing and study the perturbed steady-state wing motion. We evaluate both experiments across Weis-Fogh numbers from $1 < N < 10$. The results indicate that spring-wing systems designed for maximum energetic efficiency also experience trade-offs in agility and stability as the Weis-Fogh number increases. Our results demonstrate that energetic efficiency and wing maneuverability are in conflict in resonant spring-wing systems, suggesting that mechanical resonance presents tradeoffs in insect flight control and stability.

1. Introduction

Flapping flight is an extremely power-intensive mode of locomotion, requiring both high frequency wingbeats and large forces to produce lift and perform agile maneuvers. Flying insects achieve efficient flight through a combination of specialized flight muscles [1] and elastic energy storage in the thorax [2–4]. The insect flight system can thus be described as muscle actuation of an elastic structure which oscillates wings to generate aerodynamic forces. We call this combination of elastic, inertial, and aerodynamic mechanisms a 'spring-wing' system [5]. While significant research focus has been devoted to the aerodynamic force generation of flapping wings (see review in [6]), relatively fewer studies have focused on understanding the implications of elastic energy storage and return for flight dynamics and control [3, 4, 7–10].

In the classic spring-mass-damper model, there exists a particular actuation frequency which results in the largest amplitude oscillation of a mass, the so-called resonance frequency. In the performance considerations for a 'spring-wing' system, there exist several different resonant wingbeat frequencies at which different forms of optimality (maximum amplitude, lift, or efficiency, for example) are achieved [11]. Operating at a resonant frequency that maximizes lift can enable significant performance advantage, allowing insects to use smaller muscle force/power to generate lift for flight. Indeed, roboticists designing insect-scale flapping robots have found that incorporating elasticity and operating near resonance enables

higher lift and greater payloads using the same actuator design [8, 12–15].

To classify the relative importance of resonance in spring-wing systems we have previously introduced [5] the Weis-Fogh number (N), a dimensionless parameter that describes the ratio between peak inertial and aerodynamic torques. The Weis-Fogh number joins other important dimensionless parameters for flapping flight dynamics including the Reynolds number, Rossby number, Strouhal number, Cauchy number, and advance ratio [16–18]. The Weis-Fogh number has a mutual relationship with the Cauchy number, which in fluid-structure interaction problems represents the ratio of aerodynamic forces to elastic forces acting on a system. In the discussion we provide an analysis of how the Weis-Fogh and Cauchy numbers are related. Previous work has demonstrated that N governs how much energy can be recovered into the elastic system of insects and robots on each wingstroke, and thus is a measure of resonant efficiency for flapping wing systems [5]. However, stable and agile flight requires much more than just steady-amplitude wing oscillations, prompting the question at hand: how do spring-wing resonant dynamics impact other aspects of flight such as wingbeat control and stability?

A spring-wing system flapping at a resonance frequency is advantageous because the required power for flight is reduced. However, there are other trade-offs inherent in operating at resonance that become important for wingbeat control and stability that have not been fully considered in insect flight [19]. For example, when actuated at the resonant frequency of maximum wingstroke amplitude, any control change to the wingbeat frequency will result in a decrease in the wing amplitude and thus would require more energy input per wingstroke to achieve lift [8, 20]. Thus, while resonance can aid in energetic efficiency it can also limit the flapper's ability to quickly change wingstroke kinematics.

We hypothesize that the resonant behavior of a spring-wing system influences the insect's flapping dynamics in response to internal control changes and external perturbations. We motivate this a simple thought experiment: Consider two insects with similar wing shapes, but different total wing inertia. The insect with the larger wing inertia would have to put more energy in to driving its wing to full amplitude flapping motion. Thus, for a fixed amount of muscle force an insect with larger wing inertia—and thus larger Weis-Fogh number N—would respond more sluggishly to an amplitude control change than an insect with lower N. On the other hand, consider if the insect is flying in a crosswind and needs to maintain its wingbeat amplitude to maintain stable hovering. The crosswind is an aerodynamic perturbation that acts on the wing and may cause the wing motion to deviate from steady-state if the aerodynamic perturbation significantly overcomes the momentum of the wing motion. In the case of aerodynamic perturbations, a higher N (where inertia dominates over aerodynamic forces) would be less susceptible to wingstroke deviation. We hypothesize that the Weis-Fogh number is a governing parameter of both wingbeat response timescale (increases with N), and of susceptibility to aerodynamic perturbations (decreases with N). These two performance metrics impact maneuverability and stability in competing ways, and thus present a potential trade-off for spring-wing resonant flight.

In this study, we examine the effect that varying the Weis-Fogh number has on: (1) the responsiveness of a flapping system to a step-change in control input, i.e. starting from stop or changing amplitude, and (2) the oscillatory stability of a flapping wing subjected to an asymmetrical aerodynamic perturbation. In the first section of this work we describe the background and motivation of these hypotheses using an analytically tractable (linear) version of the spring-wing system with a viscous damper in place of aerodynamic drag. We present the results from two experiments on a dynamically-scaled spring-wing robot that measure, respectively, the time it takes for systems with different N to flap up to full amplitude and the ability of those systems to maintain sinusoidal flapping kinematics in the presence of a constant flow perturbation. In the last section we discuss the implications of these and prior results for the biomechanics of insect flight systems and the design of flapping-wing micro aerial vehicles.

2. A motivating example

In the following section, we introduce the Weis-Fogh number as a classification of spring-wing resonance. We next motivate our study's hypotheses by studying a linear spring-mass system that is subjected to a step-response change in control force amplitude, or a step-response perturbation to the damping force. Lastly, we provide a comparison between the linear spring-mass system and the nonlinear spring-wing system.

2.1. The Weis-Fogh number governs spring-wing resonance dynamics

The Weis-Fogh number is named for Torkel Weis-Fogh, a pioneer in insect flight biomechanics and discoverer of the elastic protein resilin [2, 10]. It is defined as the ratio between maximum inertial and maximum aerodynamic torque during flapping. Inertial torques are due to the acceleration of the mass of the wing and the surrounding air (added mass or 'virtual' inertia [21]) as the wing flaps, and the aerodynamic torques are due to drag on the wing in the

wing stroke plane:

$$N = \frac{\max(\tau_{\text{inertia}})}{\max(\tau_{\text{aero}})}. \quad (1)$$

If a spring-wing system has inertia I, aerodynamic drag coefficient Γ, and oscillates sinusoidally with peak-to-peak amplitude θ_o, we can express the Weis-Fogh number as

$$N = \frac{I}{\Gamma\theta_0}. \quad (2)$$

Weis-Fogh introduced this term as a part of an argument about the necessity of elastic energy storage and return in the flight system of insects [3]. It expresses the relative influence of inertial and aerodynamic effects on the dynamics of a flapping wing; $N < 1$ means aerodynamic forces dominate, whereas $N > 1$ means that inertial forces are dominant.

We found, through dimensional analysis and dynamically-scaled robotic experiments, that N also has a significant relationship to the resonant characteristics of spring-wing systems. Consider the equation of motion of a spring-wing system with structural (frequency-independent) damping as defined in [5]:

$$I_t\ddot{\theta} + k\theta + \frac{k\gamma}{\omega}\dot{\theta} + \Gamma|\dot{\theta}|\dot{\theta} = \tau_{\text{in}} \quad (3)$$

where θ is the wing angle, I_t is the total inertia of the wing plus added mass inertia, k is the average spring stiffness across the wing stroke, γ is the structural damping loss modulus [22], ω is the forcing frequency, and τ_{in} is the input torque, which is assumed to be sinusoidal for analysis purposes, The system constitutes a forced harmonic oscillator with nonlinear aerodynamic damping torque coefficient Γ, which is typically much larger than the frequency-independent structural damping term [23]. Note that this model uses bulk stiffness, inertia, damping, and torque terms that are related to multiple complex anatomical components. For example, the sinusoidal torque expression on the right hand side of the equality is a simplification of the effect of antagonistic muscles driven electrochemical signals and acting through a flexible thorax to create angular wing motion. Throughout this paper, we will focus on the bulk motion of the wing due to sinusoidal forcing and using stroke-averaged parameters to enable the reader to build intuition about these complex systems.

The expression can also be written in non-dimensional form in terms of the dimensionless angular wing displacement q, the non-dimensional stiffness $\hat{K} = \omega_n^2/\omega^2$ (which is 1 when the system is driven at its natural frequency $\omega_n = \sqrt{k/I_t}$), the structural damping factor γ, and the Weis-Fogh number N:

$$\ddot{q} + \hat{K}q + \hat{K}\gamma\dot{q} + N^{-1}|\dot{q}|\dot{q} = \tilde{\tau}_{\text{in}}. \quad (4)$$

Full derivations and further discussion can be found in [5]. Previously, we found that when flapping at resonance, the dynamic efficiency, a measure of the amount of muscle work that goes directly to producing lift/overcoming drag, $\eta = \frac{W_{\text{aero}}}{W_{\text{total}}}$, decreases as N increases in systems with any internal damping losses, i.e. from friction or viscoelastic effects [5]. Therefore, while it is beneficial to have an $N > 1$ for elastic energy exchange and resonance, higher values of N have diminishing returns in terms of peak efficiency.

2.2. Linear system analysis highlights stability and maneuverability trade-offs in resonant spring-wing flight

To gain insight into how we should expect the spring-wing to behave in our start up and constant aerodynamic perturbation experiments, we start by studying the behavior of a linear spring-mass-damper. We choose to use the linear equations because the quadratic aerodynamic damping in the spring-wing equations prohibit closed-form solutions. However, we will show that features of the linear system are analogous to the nonlinear version and draw conclusions based on that.

2.2.1. Normalized linear spring-mass-damper

Consider the normalized linear spring-mass-damper equation:

$$\ddot{x} + 2\xi\omega_n\dot{x} + \omega_n^2 x = F_m\sin(\omega t) \quad (5)$$

where ω_n is the natural frequency of the system and ξ is the damping ratio. Another way to write 5 is by defining the quality factor

$$Q = \frac{1}{2\xi} = \frac{m\omega_n}{b} \quad (6)$$

and substituting into the dynamics equation

$$\ddot{x} + \frac{\omega_n}{Q}\dot{x} + \omega_n^2 x = F_m\sin(\omega t). \quad (7)$$

The quality factor represents the effectiveness of energy storage and return in the spring-wing system during oscillations, and it can be visually represented by the 'sharpness' of the resonance peak when plotting oscillation amplitude versus frequency. Low quality factors ($Q < 0.5$) result in overdamped systems with no resonance peak and no energy savings from the spring, whereas higher Q results in a sharp resonance curve and indicates efficient energy-exchange between the spring and the oscillating mass.

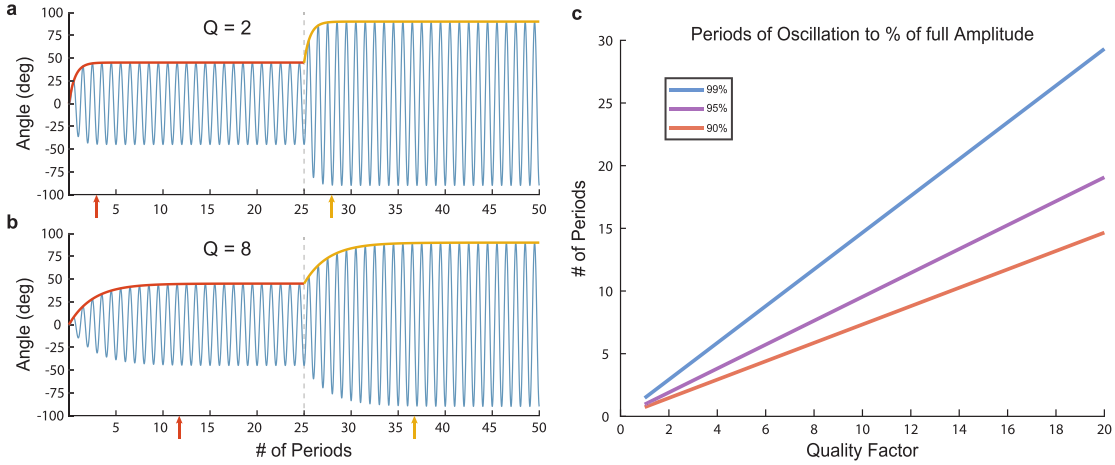

Figure 1. Rise time in simulated linear spring-mass-damper. Time to full amplitude is proportional to Q. a and b show startup to 45° degree amplitude and an amplitude change from 45° to 90° for $Q = 2$ and $Q = 8$ respectively. The rise time is slower with higher Q, as shown in c for several values of full amplitude percentage, p.

2.2.2. The time to full amplitude varies linearly with Q
The solution to the spring-mass equation (equation (7)) for $Q > 0.5$ and starting from rest is an oscillatory motion that has a transient exponential amplitude growth that saturates at the full oscillatory amplitude. The growth rate of the transient amplitude is determined from the standard methods as

$$\lambda = \frac{\omega_n}{2Q}, \tag{8}$$

which is inversely related to Q. Thus, we can solve for the time it would take a forced linear oscillator to reach ϵ =95% of full amplitude as

$$\begin{aligned} t_p &= \frac{-\ln \epsilon}{\lambda} \\ &= \frac{-2\ln \epsilon}{\omega_n} Q \end{aligned} \tag{9}$$

or, expressed in terms of the natural period $T_n = 2\pi/\omega_n$

$$\frac{t_p}{T_n} = \hat{t}_{95} = \frac{-\ln \epsilon}{\pi} Q. \tag{10}$$

This analysis tells us that transient changes in amplitude from a change in oscillator forcing will decay in a number of wingbeats directly proportional to the quality factor Q. We illustrate this phenomena in figure 1.

Thus, a spring-wing system with large quality factor will be more 'sluggish' in response to control input changes, because the response timescale is large.

2.2.3. The relative influence of aerodynamic perturbations is inversely proportional to Q
Consider a wing flapping in a viscous flow such that the effective velocity at the wing is $\dot{x} - v$. Ignoring added mass effects that may be present in the aerodynamic system, equation (7) can be rewritten

$$\begin{aligned} &\ddot{x} + \frac{\omega_n}{Q}(\dot{x} - v) + \omega_n^2 x = F_m \sin(\omega t) \\ &\rightarrow \ddot{x} + \frac{\omega_n}{Q}\dot{x} + \omega_n^2 x = F_m \sin(\omega t) + \frac{\omega_n}{Q} v. \end{aligned} \tag{11}$$

The effect of the perturbation after the transient has decayed is to introduce a torque that biases the spring in the direction of the external flow. The magnitude of the spring deflection is proportional to the flow velocity and is inversely proportional to Q. Thus the influence of an external flow on a linear flapping system is smaller in a spring-wing system with higher Q.

2.3. Resonance presents competing influences on wing maneuverability and perturbation rejection

The previous two sections illustrated how the control timescale and susceptibility to aerodynamic perturbations are influenced by the resonant properties of a linear spring-mass-damper. The quality factor (Q) is an important metric in determining properties of a resonant system, and highlights potential trade-offs in wing maneuverability and stability. Higher Q will result in a slower control response from actuation, yet external fluid forces acting on the wing will result in smaller disruption to wing motion. Lower Q will result in fast control response from actuation, however external fluid forces will cause disruption to the wingbeat kinematics. This linear systems analysis provides motivation for examining the role of spring-wing resonance in the timescales of control and susceptibility to aerodynamic perturbations in flapping wing systems.

2.4. The Weis-Fogh number N is the quality factor of a spring-wing system

One method of comparing the nonlinear spring-wing and linear spring-mass equations is to approximate the linear damping coefficient b with the aerodynamic damping coefficient Γ multiplied by the maximum velocity of the wing $\max(\dot{\theta}) = \theta_0\omega$. Defined as such, the damping terms for both spring-mass and spring-wing equations are equivalent at mid-stroke where the wing velocity is highest. This is called the secant approximation and has been used in previous analysis of flapping wing systems [24]. We can define the following relationship for the linear damping coefficient that models the spring-wing

$$b_{\text{sw}} = \Gamma\theta_0\omega. \tag{12}$$

Substituting this expression into the equation for the damping ratio yields the following

$$\begin{aligned}\xi &= \tfrac{b_{\text{sw}}}{2m\omega_{\text{n}}} \\ &= \tfrac{\Gamma\theta_0\omega}{2m\omega_{\text{n}}} \\ &= \tfrac{1}{2N}\tfrac{\omega}{\omega_{\text{n}}}.\end{aligned} \tag{13}$$

Thus, we see that the Weis-Fogh number has a natural connection to the damping ratio of a linear spring-mass system under the secant approximation. If we make the assumption that the system is on resonance ($\omega = \omega_{\text{n}}$) then the relationship is as follows

$$\xi = \frac{1}{2N}. \tag{14}$$

We can push this analogy one step further if we consider how the quality-factor relates to the damping coefficient, and by extension the Weis-Fogh number

$$\begin{aligned}Q &= \tfrac{1}{2\xi} \\ &= \tfrac{2N}{2} \\ &= N.\end{aligned} \tag{15}$$

We have demonstrated that the Weis-Fogh number is equal to the quality factor of a linearized spring-wing system using the secant approximation. This corresponds to our measurements in [5].

We test the scaling relationship between Weis-Fogh number N and the dynamic behavior of spring-wings via two experiments in a robophysical model. The first measures response to control inputs by measuring time to peak amplitude from rest, and the second measures the effect of environmental perturbations via measuring the effect of constant cross-flow on symmetry of flapping dynamics. The results suggest that in addition to its effect on peak dynamic efficiency, N illustrates the scaling of agility and perturbation rejection among insects and other small-scale flapping systems.

3. Experimental methods

To demonstrate the relationship between N and the tradeoffs in stability and agility of flapping in spring-wing systems, we perform a series of experiments on a dynamically-scaled robotic spring-wing system. The robotic system is subject to real fluid forces at Reynolds numbers that are scaled to those experienced by insects and insect-scale robots.

3.1. Dynamically-scaled, series elastic robophysical model

The robotic spring-wing system used in this paper was described in detail in [5] and is shown in figure 2. It consists of a high-torque servo motor (Teknic ClearPath) connected to a rigid, fixed pitch acrylic wing in a large tank of water. The elasticity comes from a molded silicone torsion spring in series with the wing 2. We created three springs from Dragon Skin 30 silicone (SmoothOn) cast in 3D printed molds, varying the geometry so that they each had a different stiffness. We vary the overall inertia of the system by attaching mass to the main shaft of the flapper (above the water) in the form of acrylic and aluminum plates (figure 2(c)). We minimize friction by integrating radial air bearings and a thrust ball bearing, and we assume that drag from rotation through the air is much smaller than from the motion of the wing in water. See table 1 for a list of the inertia and stiffness values.

3.2. Controlling N, an emergent property of spring-wing flapping systems

We sought to compare the transient behavior of the flapper when it flaps with different values of N. However, due to the dependence on flapping amplitude θ_0, N is an *emergent* quality of a system, and therefore is difficult to prescribe directly. The following section describes the process of determining robotic system configurations for a range of $N = 1$–10 that are used for robustness and agility experiments. In all cases, we refer to a value of N computed using the steady-state flapping amplitude, θ_0, and the mean drag torque coefficient Γ at steady state.

3.2.1. Determine constraints

Based on the range of N seen in insects and flapping robots [3, 5], we sought to test 10 integer values of N, from $N = 1$ to $N = 10$. Since we are interested in resonant flapping performance, we require the forcing frequency be at the damped resonant frequency,

$$\omega_{\text{r}}^2 = \frac{\omega_{\text{n}}^2}{\sqrt{1 + 4N^{-2}}}, \tag{16}$$

derived using the method from [5]. Additionally, we seek to minimize the range of Reynolds number (Re) across tests. The roboflapper is designed to operate within a range of Re that is similar to insects and small birds ($Re \in [10^2$–$10^4]$), as significant deviations out

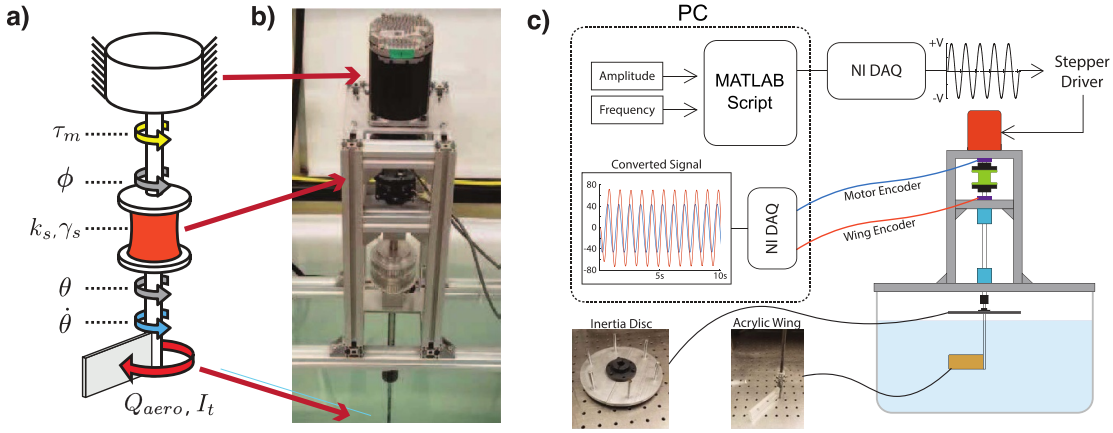

Figure 2. The series-elastic spring-wing system. (a) Conceptual diagram indicating the angle input, linear spring with structural damping, and rigid fixed-pitch wing. (b) Corresponding photo of the roboflapper indicating the ClearPath servo motor, silicone torsion spring, and acrylic wing in a large tank of water. (c) Diagram of the whole electromechanical system. Reproduced from [5]. CC BY 4.0.

Table 1. Inertia and spring stiffness values for the roboflapper.

Inertia (kg m^2)		Springs (Nm rad^{-1})	
IA	0.00 105	K1	0.164
IB	0.00 149	K2	0.416
IC	0.00 233	K3	0.632
ID	0.00 476		

of that range introduce aerodynamic phenomena that may not be relevant to flapping flight at that scale.

Beyond those considerations, we are limited by constraints on the robotic system. Mechanically, we must use one of three silicone springs, one of four discrete inertial configurations, and the same wing with $\Gamma = 1.07 \times 10^{-3}$ Nm. On the control side, we found that our system works best when the flapping amplitude is between ~30° and 120° peak-to-peak and the flapping frequency is between 0.5 and 3 Hz.

3.2.2. Choosing configurations for values of N

With three springs and four inertia configurations, we have a total of 12 combinations of springs and inertia plates that are possible. We have continuous control of the amplitude and frequency within functional bounds. The process of choosing a configuration for each value of N is as follows:

(i) Given a particular value of N, compute $\theta_o = \frac{I}{\Gamma N}$ for each of the four inertias. Exclude any configuration where $\theta_o > 60°$.

(ii) Compute the resonant frequency f_r based on the remaining inertias and the three available springs. Exclude any configurations where f_r is greater than 3 Hz or less than 1 Hz.

(iii) Compute the Reynolds number, $Re = \frac{\bar{U}_{tip}\bar{c}}{\nu}$, of flapping based on that amplitude and frequency as well as wing length and chord, 10 cm and 3.6 cm, respectively. Exclude configurations with $Re > \approx 15\,000$, which is near upper limit of Reynolds number for insects and hummingbirds [18].

(iv) Select a configuration for each value of N from the non-excluded configurations

The final selections are given in table 2.

3.3. Experiment 1: starting from rest and changing amplitude

We sought to measure the effect of a system's N on the time it takes for the system to respond to a change in input forcing amplitude. A straightforward way of doing so is to measure the time it takes for flapping oscillations to reach a steady-state amplitude after startup. Furthermore, we measured the time it takes to reach a new amplitude after a change in the input.

For each test, the spring stiffness and inertia were set based on the configurations above. The system was driven by a sine wave position signal to the servo through Simulink Desktop Real-Time (Mathworks) and a PCIe 6343 interface (National Instruments). The frequency was set based on the configuration table, but the wing amplitude is not set explicitly because of the series-elasticity of the roboflapper. We found previously that modeling does not fully predict the kinematic gain between angular motor amplitude and wing amplitude [5]. Therefore, for each configuration, we found the proper input amplitude to achieve the desired wingbeat amplitude iteratively using a separate Simulink Desktop Real-Time program, prior to the tests, and recorded the input amplitudes. When we performed each experiment, we used the input amplitudes to drive the system in open-loop, which was a fairly reliable way to dictate N (see table 2).

Each test was performed by starting the sinusoidal position signal and running for 15 flapping periods, long enough for the amplitude to stabilize (figure 3(a)). After 15 periods, the sinusoidal amplitude of the motor position command signal was

Table 2. Spring, inertia, target amplitude, and frequency configurations for each experiment. Amplitude is given as half of the peak-to-peak stroke. The rightmost column lists the mean and standard deviation of the emergent value of Weis-Fogh number, N, for each configuration based on the flapping amplitude measured via a sine curve fit.

Exp.	Spring	Inertia	Amplitude (deg)	Frequency (Hz)	N
1	K1	IA	56.2	1.33	1.0 ± 0.01
2	K1	IB	40.0	1.40	2.0 ± 0.01
3	K2	IA	18.7	2.89	3.0 ± 0.01
4	K2	IB	20.0	2.51	4.0 ± 0.01
5	K2	IC	25.0	2.05	5.0 ± 0.04
6	K3	ID	42.5	1.45	6.0 ± 0.01
7	K3	ID	36.8	1.45	6.9 ± 0.02
8	K3	ID	31.8	1.80	8.0 ± 0.02
9	K3	ID	28.3	1.81	9.0 ± 0.03
10	K3	ID	25.5	1.82	10.0 ± 0.03

increased by 50%, and the experiment continued for a further 15 periods before ending the experiment. This process was repeated five times for each value of N and sampled at a rate of 1000 samples per period. Note that we refer to the number of periods and that each experiment was run at a different frequency (table 2), so the total runtime varied. The final amplitude θ_0 was determined by fitting a sine curve to the last 5 periods of the each portion of the test using a bounded nonlinear least squares method in MATLAB (Mathworks). Then an exponential curve ($f(t) = \theta_0(1 - e^{-\lambda t})$ was fit to the peaks of absolute value of the wing angle in the start and step portions of the data, and the time to 95% of θ_0 was computed using $\hat{t}_{95} = -\ln(0.05)\lambda^{-1} f_r$ (figures 3(b) and (c)). To create the plots in figures 3(b) and (c), N was recalculated based on actual experimental amplitude measurements using equation (2). The actual amplitude from fitting the sine curve varied slightly from the prescribed amplitude, resulting in a small amount of horizontal spread of effective N for each experiment. The means and standard deviations of both N and $\hat{t}_{95}$ are plotted in appendix B, and the values for N can be found in table 2.

3.4. Experiment 2: effect of constant cross-flow

For the second experiment, we wanted to see how N relates to the flapping wing's ability to reject environmental disturbances. We did this by subjecting the flapping wing to a constant crossflow and measuring its deviation from a symmetrical sine wave. The flow was provided by a submerged aquarium pump (Simple Deluxe LGPUMP400G 400 GPH) fitted with a 1/2" diameter rubber tube. The outlet of the tube was positioned such that it was aligned with the acrylic wing in the tank and created the maximal passive deflection (see figure 4(a) against the spring, but did not interfere with flapping, i.e. there was no difference between flapping trajectory whether the tube was in place or not. We measured the torque on the wing when the pump was on and the flow was perpendicular with the wing. We found that the torque was approximately 0.01 Nm, only enough to deflect the softest spring about 3.5°. The maximum peak aerodynamic torque across the experiments is for $N = 1$ and is $\tau_{amax} = \Gamma(\theta_0)^2(2\pi f)^2 = 0.072$ mNm. Thus the magnitude of the perturbation is significantly lower than the maximum drag induced by flapping motion, but is still enough to induce asymmetry in flapping.

We ran the flapper with a constant sinusoidal input that produced a wing amplitude consistent with the proper configuration at each value of N. We recorded the wing trajectory with the pump off to set a baseline at each value of N, then turned the pump on. We analyzed the impact of aerodynamic perturbation on the flapping kinematics by fitting a sine function to the wing trajectory at steady state using MATLAB functions (Mathworks) and recording the fit error (RMSE). The fit error was normalized to the flapping amplitude at that configuration so that it represents the fraction of flapping amplitude and is unitless. Additionally, we noted a change in steady flapping amplitude with the pump on, and plotted the relative change in amplitude from the no flow case to the constant flow case.

4. Results

4.1. Start time and step time increase linearly with N

We measured the time interval from initiation of flapping to reaching 95% of the steady-state flapping wing amplitude from an exponential fit. To normalize this time period across different resonance frequencies we multiplied the start-up time by the frequency of flapping, resulting in a measurement of the number of wing strokes to reach steady-state. The results across N are shown in figure 3(b). We see that there is a clear relationship between increasing N and increasing time to full amplitude (dashed lines). Configurations with $N = 1$ or 2 are at full amplitude within a single wingstroke, whereas $N = 8$–10 systems take four or more wingstrokes.

The relationship is linear ($t_{start} = 0.486N - 0.243$), but there is a small amount of variance (appendix, figure B1) for each prescribed value of

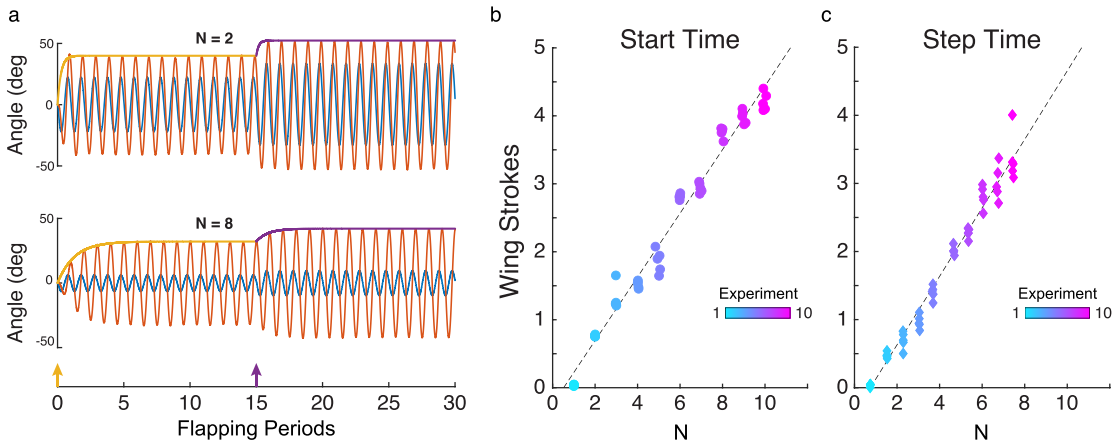

Figure 3. Responsiveness Experiments. (a) We drive the series-elastic system via servo (blue) and measure the emergent flapping kinematics (orange). We fit exponential curves to the flapping peaks during start up (yellow) and after an input step (purple) 15 cycles after start. The measured time (in wing strokes) to full amplitude is linearly related to N (b & (c). However, the effective value for N is less than prescribed after the step due to an increase in flapping amplitude (c).

N. The vertical spread is to be expected due to fitting in the presence of noise, but we also found that the rise time was sensitive to whether or not the system was at exactly the resonant frequency, maximizing the kinematic gain ($G_k = \theta_o/\theta_{input}$). This was a more significant issue at higher N because of the steeper resonant curve, and the added mass of the system would have made it susceptible to small asymmetries and potentially larger friction, though that was mediated by thrust ball bearings. The horizontal spread indicates that we were not always *exactly* at the desired value of N. The means and standard deviations of N from 1 to 10 are shown in table 2, and the standard deviations are illustrated by the horizontal bars in figure B1.

The response time after a step increase in input also has a clear linear relationship with N (figure 3(c)). The linear fit is slightly different from the startup data ($t_{start} = 0.503N - 0.376$), but they largely fall upon the same line. The major difference between the two is that because of the change in amplitude after the step, the effective value of N is lower than it was before the step due to the inverse relationship between θ_0 and N (equation 2). The effect is a compression of the datapoints along the diagonal, since the response time decreases along with N, as shown in figure 5.

4.2. Resistance to perturbations increases with increasing N

We subjected a flapping wing at steady-state amplitude to a transverse flow, and we measured the change in wingstroke kinematics after flow onset. We observed that spring-wing configurations with larger Weis-Fogh number sustained sinusoidal flapping wing kinematics in the presence of flow perturbations, whereas lower N systems exhibited a distortion in the sinusoidal wing motion (figure 4). This asymmetrical warping of the wing trajectory at low N was observed as non-sinusoidal wing kinematics (4(a)) and a corresponding non-circular phase portrait (figures 4(a) and (b)). Note that the trajectories are 'lumpier' when N is small, but also that there's a decrease in flapping amplitude overall at higher N.

We fit a sine wave to each trajectory and calculated the root mean squared error (RMSE) relative to the flapping amplitude, which quantifies how well a sine wave fits to the data. This error will never reach zero, but for the no-flow case, it is small—just 0.76% of the flapping amplitude. We find that the sinusoidal fit error at $N = 1$ is approximately ten times larger than for $N \approx 10$ with a maximum error near 8% of the flapping amplitude.

Based on equation (11) and our association of Q and N, we expect that the influence of asymmetric flow should be inversely proportional to N. We fit an inverse curve $AN^{-1} + C$ to the error data, fixing the offset $C = 0.0076$ to be equal to the measured baseline no-flow error. The optimal curve ($P_{lin}(N) = 0.053N^{-1} + 0.0076$) based on the linear analysis does a fairly poor job of fitting the data ($R^2 = 0.80$). Thus we relaxed the constraint on the power of N and fit the curve $AN^{-B} + C$, which produced a curve ($P_{lin}(N) = 0.073N^{-1.745} + 0.0076$) that fit the data much more closely ($R^2 = 0.97$). We also measured the final amplitude while the flow was turned on for each experimental configuration and compared to the initial amplitude at that value of N. We found that the amplitude was reduced by an average of 16.4%, regardless of N. This is unlike the expectation from the linear damping case, where we would not expect to see a decrease in amplitude, just a shift in the center of oscillation.

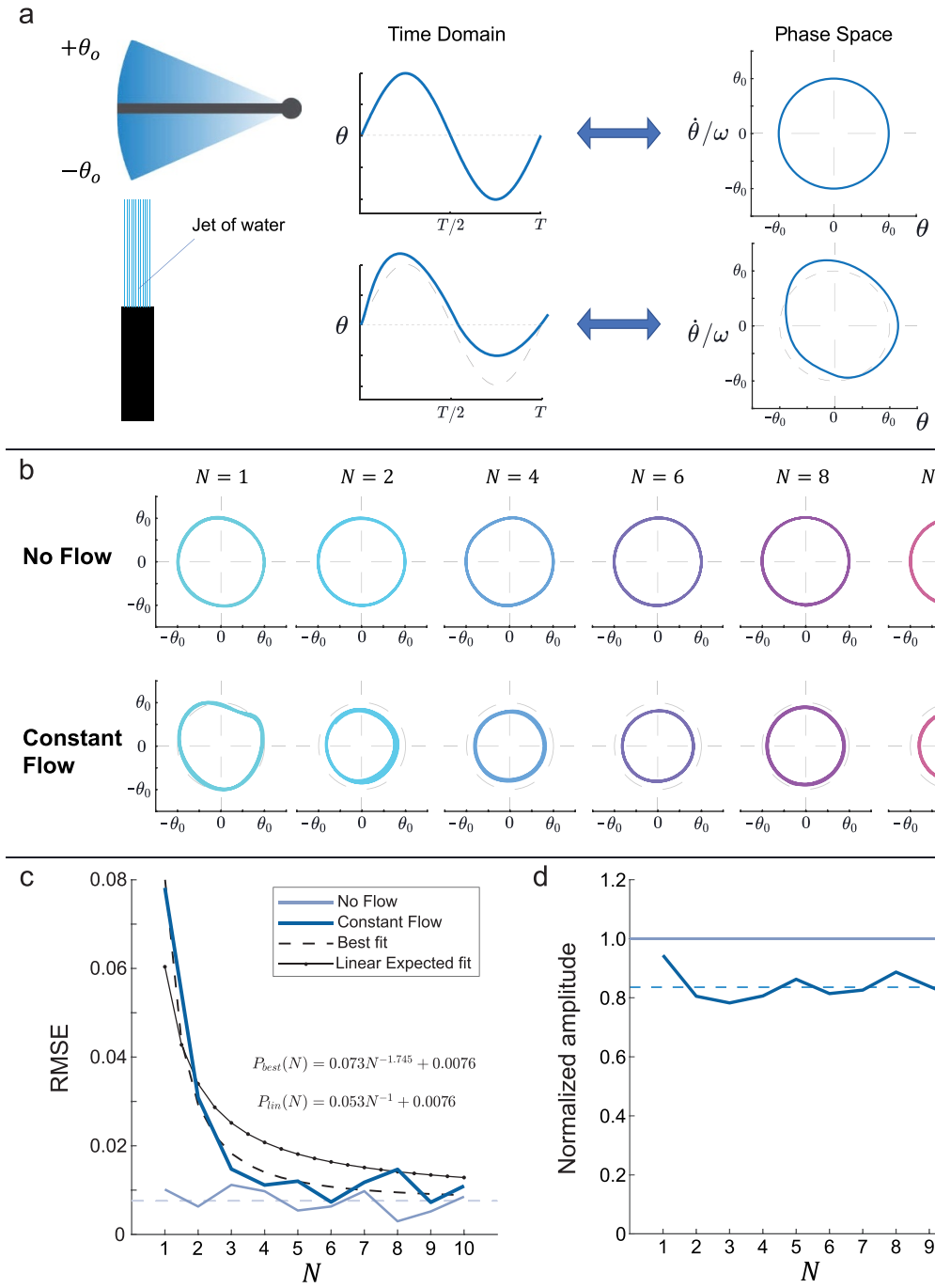

Figure 4. Description of the constant flow experiments. (a) Schematic of the orientation of the water jet relative to the wing, and conceptual representation of the effects of flow on time and phase domain plots. (b) Variation in limit cycle plots across N. Plots show 2 periods of steady oscillation with and without flow, at different values of N. (c) Plots of fit error for flow and no-flow cases across N, as well as fit lines for expected N^{-1} function and a best fit curve. (d) Illustration of relative amplitude decrease across N, and mean at 84% of full amplitude.

5. Discussion

5.1. Lower N provides faster responsiveness to wingbeat amplitude control changes

We have shown that the time it takes for a spring-wing system to respond to a control input change is linearly related to Weis-Fogh number, N. Thus a flyer with a greater Weis-Fogh number—determined by their wing mass, wing shape, wing-stroke kinematics, and wing pitch kinematics—will have reduced control authority when it comes to starting, modulating, or stopping wing motion. In order to perform high-speed agile maneuvers, insects need to be able to quickly modulate lift and drag forces. They can do so by modulating both amplitude and frequency [19], but more often at higher frequencies it is accomplished by modulating wing rotation [25, 26]. The modulation of wing angle of attack or joint characteristics via steering muscles [27] may be more effective at high N since they can modulate both

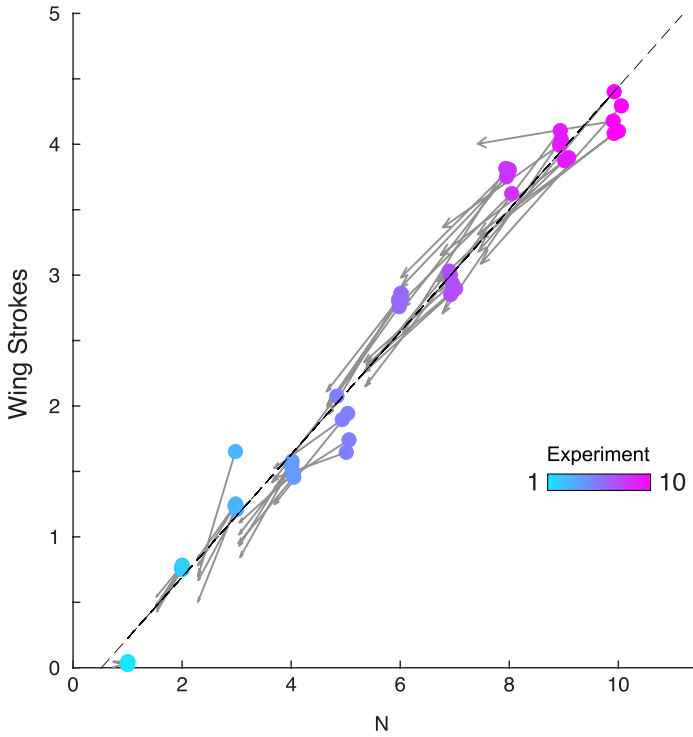

Figure 5. Amplitude increases due to a step increase in input amplitude lead to commensurate decreases in N and transient time. Data points are shown in color, and gray arrows indicate the movement due to increased control input. The arrows are all roughly aligned with the trendline.

amplitude *and* Weis-Fogh number by changing the aerodynamic characteristics of the wing. Our input step experiments demonstrate that, since N is a function of flapping amplitude, changes to amplitude also change the control authority. Figure 5 shows the degree to which N and transient time shift due to the increase in amplitude. The arrows start at the points corresponding to the startup time and point to the location in the plane where the step time is located. The arrows follow the linear trendline, and the length of the arrow is greater for larger starting values of N. In engineering, control authority is critical for ensuring that a system can meet performance objectives like stabilization in the presence of disturbances or trajectory following. The loss of control authority—stalling in an airplane, for example—can lead to catastrophic failure if control is not regained in time. In insects, the ability to quickly maneuver through an array of obstacles or out of the grasp of a predator is similarly important. Since N is relatively easy to measure for a particular species of insect, requiring just estimates of wing mass, wing shape, and wing kinematic data, it may serve as a useful metric for an insect's relative ability to perform agile maneuvers. Additionally, it suggests an opportunity for new designs of flapping robots that incorporate control via wing pitch modulation that could enable dynamic modulation of control authority based on control objectives.

5.2. Higher N provides greater stability in unpredictable natural environments

An insect or flying robot that needs to be more agile may benefit from a lower N, but there is a tradeoff of wing stroke stability. At lower N, the inertia of the wing during flapping is of the same order as the aerodynamic forces, so variations in aerodynamic forces from the environment (turbulence, wind gusts, etc) will have a larger effect on the flapping wing kinematics. This can pose issues for an insect, since steady wingbeats are necessary to produce consistent lift. Our flow experiments show that an insect or flapping wing robot with body elasticity is less susceptible to disruptions from the environment when it has a high Weis-Fogh number. This means that a flapper that needs to fly in a windy environment may benefit from lower amplitude flapping, more massive wings, and/or wing shapes or stroke profiles that minimize drag.

5.3. Weis-Fogh number as the quality factor of spring-wing systems

The series of analyses we performed in the first section of this paper looking at the transient behavior of a linear spring-mass-damper as an analogue to the spring-wing system illustrate that the quality factor Q is linearly related to the startup time of the system and inversely related to the relative effect of external perturbations. Our experimental results

with the nonlinear spring-wing system show similar trends.

5.3.1. Changing amplitude changes the transient time constant

As shown in figure 5, the response time of the spring-wing to a control input depends not just on the magnitude of the input, but also on the amplitude of flapping. This is an inherently nonlinear phenomenon due to aerodynamic damping, and is not the case for the linear system. However, since the shift induced by the amplitude change (gray arrows, figure 5) follows the trendline fairly closely, it does seem that the relationship between N and response time is maintained despite the transient changes in N.

The actual relationship we expect between response time (defined at 95% of the full amplitude) and Q based on equation (10) is

$$\hat{t}_{95} = \frac{-\ln 0.05}{\pi} Q = 0.9536Q \approx Q. \tag{17}$$

If we inspect the trendline for the response time of the spring-wing system we find the relationship

$$\hat{t}_{95} = 0.486N \approx \frac{N}{2}. \tag{18}$$

Thus, we find that the response time of an oscillator to control commands scales linearly with the Weis-Fogh number in the case of flapping wings and with the quality factor in the case of a linear spring-mass-damper.

This finding agrees qualitatively with the relationship shown in equation (16), but notably, other methods of linearizing the aerodynamic force will produce different proportionality relationships. For example linearization can be done by equating the energy dissipation between an aerodynamic and a viscous force. However, prior comparisons between quality factor and Weis-Fogh number are consistent with our findings of a proportional (linear) relationship between Q and N, with differing proportionality constants depending on the assumptions [10, 11, 28].

5.3.2. Nonlinear aerodynamics results in more stability at higher N

In section 2, we argued that an external flow should affect a linear spring-mass-damper less as Q increases, i.e.

$$F_{\text{flow}} = \frac{\omega_n}{Q} v. \tag{19}$$

Thus we expected an inverse relationship between N and flapping non-sinusoidality. Additionally, we expected that a flow should cause a consistent off-center stretch in the spring, i.e. a steady-state offset in the positive x direction (equation (11)), but maintain the same flapping amplitude.

In fact, we found that an inverse (N^{-1}) relationship did not fit the data well. Instead, a function with $N^{-1.745}$ fit better, suggesting that the quadratic relationship between the system and the flow asymmetry, $\Gamma|\dot{x} - v|(\dot{x} - v)$, introduces dynamics that result in greater passive stabilization of the sinusoidal wing kinematics. Additionally, we see that the flapping amplitude *is* affected by the asymmetry, causing a decrease in overall amplitude. This would be detrimental to a high-N flapping flyer's ability to produce lift, but as long as it is not using maximum muscle strength during normal flapping, it should be able to increase the force it uses to drive the wings to achieve the necessary amplitude. The situation would be worse for a low-N flyer which would need to control amplitude variations within a single wingstroke to maintain smooth flapping, regardless of the strength of the muscle

5.4. Weis-Fogh number as a performance metric for flapping fliers—living or engineered

In this and previous experimental and theoretical work [5, 10], we have shown that the Weis-Fogh number is a metric that encompasses important performance characteristics for flapping flight: dynamic efficiency, responsiveness/agility, and stability. When we plot the distribution of Weis-Fogh Number across a wide range of insects, large and small, we notice that they seem to exist in the range of $N =$ 1–8. There are some exceptions, of course, but they are characterized by the extremely small flying insects [29] who fly at very low Reynolds numbers, and butterflies, whose especially large wings and stuttering wing stroke dynamics distinguish them from the more controlled hovering of flies, bees, and hawkmoths. Small insects like those studied in [29] likely have values of $N << 1$ (*Paratuposa placentis*, $N \approx 0.14$, see appendix) due to the presence of bristled wings that significantly decrease wing inertia, and therefore drive N to be smaller; butterflies, like *Pieris Brassicae*, $N \approx 0.4$, also have $N < 1$, but via large aerodynamic drag from large wings. Since the benefits of elastic energy storage drop off when $N < 1$, we would expect that such insects need to develop adaptations other than thorax elasticity to maintain flight. However, thorax elasticity is critical when flight requires wings with significant inertia and high frequency wingbeats. The fact that other insects who rely on fast wingbeats exist in this constrained range of Weis-Fogh number suggests that the variation in N may reflect a balance of different performance trade-offs (figure 6).

Similarly, mechanical system parameters can reflect trade-offs between agility and stability. Fighter aircraft with adjustable wings are one example of a system that can shift from a more stable shape (wings extended) to a faster, more agile, but less stable configuration (wings folded). This has been taken to an

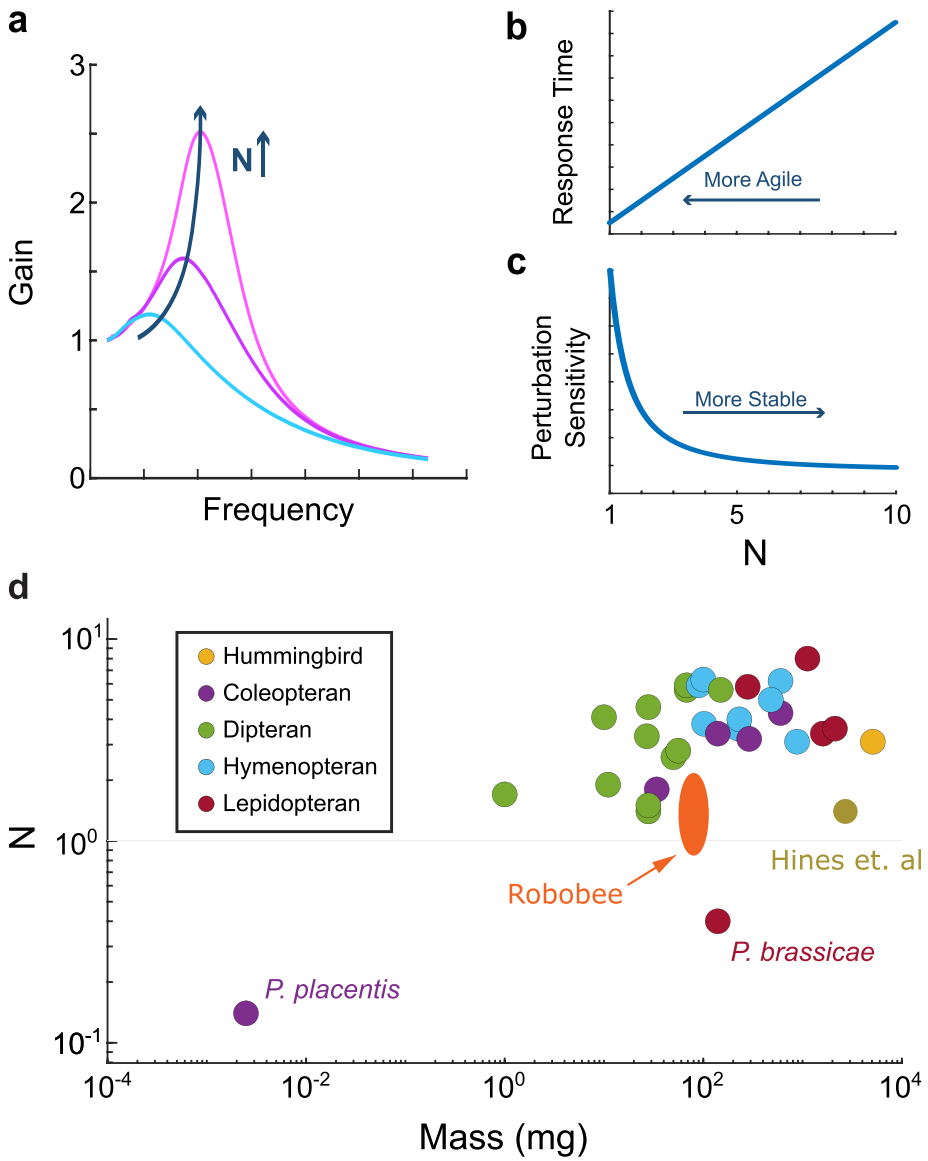

Figure 6. Flapping system performance trade-offs. (a) Higher N means greater flapping amplitude for a given actuator. (b) Lower N leads to faster response times, but (c) more vulnerability to aerodynamic perturbations. (d) This may point to an explanation for the number of insects and flapping micro-aerial vehicles [30] across orders of magnitude of size that remain within the range of $N = 1$–8. Low-N exceptions like *Paratuposa placentis*[29] and *Pieris brassicae* [3] may point to unique adaptations for efficient flight.

extreme with fighter jets with forward-swept wings, like the Grumman X-29, which trades off high maneuverability for increased instability. Indeed, there is even some evidence that wing morphing in birds similarly leverages aerodynamic instability to improve flight performance [31].

Thus it makes sense that the evolutionary development of flapping flight should also balance energetics, agility, and stability. Perhaps the restriction of flapping animals to a moderate region of Weis-Fogh number ($N =$ 1–8) is due to tradeoffs that occur between 1) energetic efficiency (increases with N), 2) wing stroke responsiveness to control inputs (decreases with N), and 3) passive wingstroke stability when subjected to external perturbations (increases with N). Those, combined with the necessity of elastic energy exchange to maintain efficient flight, may constitute a driver of evolutionary change.

6. Conclusions

The evidence presented in this manuscript and our prior work [5] suggests that the Weis-Fogh number, an underappreciated non-dimensional parameter first identified by Torkel Weis-Fogh in the 1970's, is an indicator of several important aspects of flapping flight [2, 10]. Determining the Weis-Fogh number of a flapping wing system—be it biological or robotic—can provide insight into the system's ability

to benefit from elastic energy storage and release, perform agile maneuvers by modulating their wingstroke kinematics, and deal with aerodynamic perturbations while maintaining a stable hover. However, this is just the first step to understanding 'spring-wing' system dynamics. Further work is necessary to understand how insects leverage resonant dynamics and better understand how to design high-performance flapping robots.

For example, while this work has focused on flapping at or near resonance, recent studies have complicated the picture of resonant flapping flight in insects. In two studies, Pons and Beatus [11, 28] found that, in systems with both parallel and series elasticity such as the flight anatomy of flies, multiple separate resonance frequencies may exist, creating 'band' resonance where resonance benefits may occur over a broad range of flapping wing frequencies. In biological measurements of the flight anatomy of 10 species of Bombycoid moths, Wold found that each species flapped its wings not at its resonant frequency, but at a significantly higher frequency [9, 10]. That study found that insects with Weis-Fogh numbers that would enable efficient flight at resonance seem not to leverage that energetic benefit, instead flapping at higher frequencies, for reasons that are not yet fully understood. Additionally, the dynamics of many insects are heavily influenced by self-excited asynchronous flight muscle, blurring the definition of 'resonance' and complicating the spring-mass-damper analogy. Flapping frequency in these self-excited systems is an emergent property that depends on not only the mechanical aspects of the anatomy, but also the timing and strength of myogenic force production in the muscles [32].

Another aspect of resonant flight that begs more study is the influence of wing pitch and wing flexibility. Here, we have used a rigid plate to emulate a wing, and we do not vary the pitch angle during flapping. However, studies have found that wing flexibility can lead to improved flight efficiency via elastic energy storage [33] and beneficial fluid-structure interactions. The aeroelastic interactions between a wing membrane and the fluid are far more complicated than the single degree of freedom presented here, and today many studies of flexible wing structures lean on computational fluid dynamics methods or dynamical scaling approaches. Dynamically scaling a continuum fluid-structure interaction problem like a bending flexible wing can be complicated because it requires matching several dimensionless parameters like the Reynolds number, the Cauchy number, the mass number, and the Strouhal number [16, 17]. The Cauchy number represents the ratio of fluid dynamic forces to elastic forces exerted on a structure. In the context of our one-dimensional spring-wing system it is interesting to examine the Cauchy number (Ch). In our experiments we drive the wing at resonance and thus the maximum inertial forces at resonance are equal to the maximum elastic forces and thus by inserting this into the Cauchy number definition we find that

$$Ch = \frac{\max\left(\tau_{\text{aero}}\right)}{\max\left(\tau_{\text{inertia}}\right)} = \frac{1}{N}. \tag{20}$$

Thus, by scaling our experiment to match the range of calculated Weis-Fogh numbers for insects and scaling Reynolds number appropriately we are able to dynamically match the spring-wing dynamics of insects.

This work has the potential to impact future biological and robotics studies of flapping wing flight. Future robophysical and robotic experiments could investigate the interactions between body and wing elasticity or seek to understand how sub-wingstroke modulation of wing pitch or stroke plane may enable agile maneuvers despite average wingstroke dynamics that have a high Weis-Fogh number. Such studies would further deepen our understanding of the environmental and evolutionary pressures that drive morphology and also drive innovation in the design of flapping wing robots. Furthermore, the control of flapping wing motion is challenging, and studies could seek better understanding of how to incorporate beneficial system elasticity not just for efficiency gains but also for control and stability purposes. Overall, elasticity is present and important in the insect flight system and future investigations will benefit from a focus on understanding the interaction between actuators, elastic elements, and aerodynamic forces.

Data availability statement

The data that support the findings of this study are openly available at the following URL/DOI: http://datadryad.org/stash/share/aeycYaVp3-Lv8q3nzz42z2dntDRF80LGp5Fc4NNvMTY.

Acknowledgments

This work was supported by US National Science Foundation RAISE Grant No. IOS-2100858 to S S and N G and 1554790 (MPS-PoLS) and a Dunn Family Professorship to S S as well as the US National Science Foundation Physics of Living Systems SAVI student research network (GT node Grant No. 1205878).

Appendix A. Computing N using measures of flapping power

When the maximum aerodynamic and inertial torques are not available to compute the Weis-Fogh

number, it is also possible to approximate using the aerodynamic and inertial power. Note, this approximation assumes sinusoidal wingstrokes, which is far from guaranteed; however, this gives a first-order approximation that can be improved through deeper analysis.

Given a sinusoidal wing trajectory $\phi = \phi_o \sin(\omega t)$, the inertial and aerodynamic torques on the wing, according to 3, are

$$T_\mathrm{i} = I\ddot{\phi} = -I\phi_o\omega^2 \sin(\omega t) \tag{A.1}$$

$$T_\mathrm{a} = \Gamma|\dot{\phi}|\dot{\phi} = \Gamma|\phi_o^2\omega^2|\cos(\omega t)\,|\cos(\omega t)\,. \tag{A.2}$$

The respective inertia and aerodynamic powers are therefore

$$\begin{aligned} P_\mathrm{i} = T_\mathrm{i}\dot{\phi} &= \left(-I\phi_o\omega^2 \sin(\omega t)\right)\phi_o\omega\cos(\omega t) \\ &= -0.5I\phi_o^2\omega^3 \sin(2\omega t) \end{aligned} \tag{A.3}$$

$$\begin{aligned} P_\mathrm{a} = T_\mathrm{a}\dot{\phi} &= \left[\Gamma\phi_o^2\omega^2|\cos(\omega t)\,|\cos(\omega t)\right]\phi_o\omega\cos(\omega t) \\ &= \Gamma\phi_o^3\omega^3|\cos(\omega t)\,|\cos^2(\omega t)\,. \end{aligned} \tag{A.4}$$

The maximum magnitudes are $|P_\mathrm{i}|_\mathrm{max} = 0.5I\phi_o^2\omega^3$ and $|P_\mathrm{a}|_\mathrm{max} = \Gamma\phi_o^3\omega^3$. Therefore,

$$\frac{|P_\mathrm{i}|_\mathrm{max}}{|P_\mathrm{a}|_\mathrm{max}} = \frac{0.5I\phi_o^2\omega^3}{\Gamma\phi_o^3\omega^3} = \frac{I}{2\Gamma\phi_o} = \frac{N}{2} \tag{A.5}$$

and

$$N = 2 \times \frac{|P_\mathrm{i}|_\mathrm{max}}{|P_\mathrm{a}|_\mathrm{max}}. \tag{A.6}$$

We use this estimate of N to plot the featherwing beetle *Paratuposa placentis* alongside the reported values of N from Weis-Fogh [3]. Based on this relationship, we can inspect figure 3(e) from [29] and see that there is a maximum (mass specific) aerodynamic power of ~110 W kg^{-1} and inertial power of ~7.8 W kg^{-1}. Thus $N \approx 0.14$. We were able to place it on the chart in figure 6(e) using the fact that the reported body mass is 2.43 ± 0.19 μg [29].

It is also possible to compute N from mean values of P_i and P_a, as opposed to maxima. In that case, we integrate the expressions for P_i and P_a over the portion of the wingstroke where they are both positive (the first half of the half-stroke):

$$\bar{P}_\mathrm{i} = \int_0^{\frac{\pi}{2\omega}} 0.5I\phi_o^2\omega^3 \sin(2\omega t)\,\mathrm{d}t = \frac{1}{2}I\phi_o^2\omega^2 \tag{A.7}$$

$$\bar{P}_\mathrm{a} = \int_0^{\frac{\pi}{2\omega}} \Gamma\phi_o^3\omega^3|\cos(\omega t)\,|\cos^2(\omega t) = \frac{2}{3}\Gamma\phi_0^3\omega^2. \tag{A.8}$$

We can then relate N to the ratio of these values:

$$\frac{\bar{P}_\mathrm{i}}{\bar{P}_\mathrm{a}} = \frac{\frac{1}{2}I\phi_o^2\omega^2}{\frac{2}{3}\Gamma\phi_0^3\omega^2} = \frac{3}{4}\frac{I}{\Gamma\phi_0} = \frac{3}{4}N. \tag{A.9}$$

Thus we can take measurements of mean inertial and aerodynamic power, such as that reported by Ellington [34], and compute N using the relationship $N = \frac{4}{3}\frac{\bar{P}_\mathrm{i}}{\bar{P}_\mathrm{a}}$. We have included data from [34] calculated in this way in figure 6.

Appendix B. Additional tables and figures

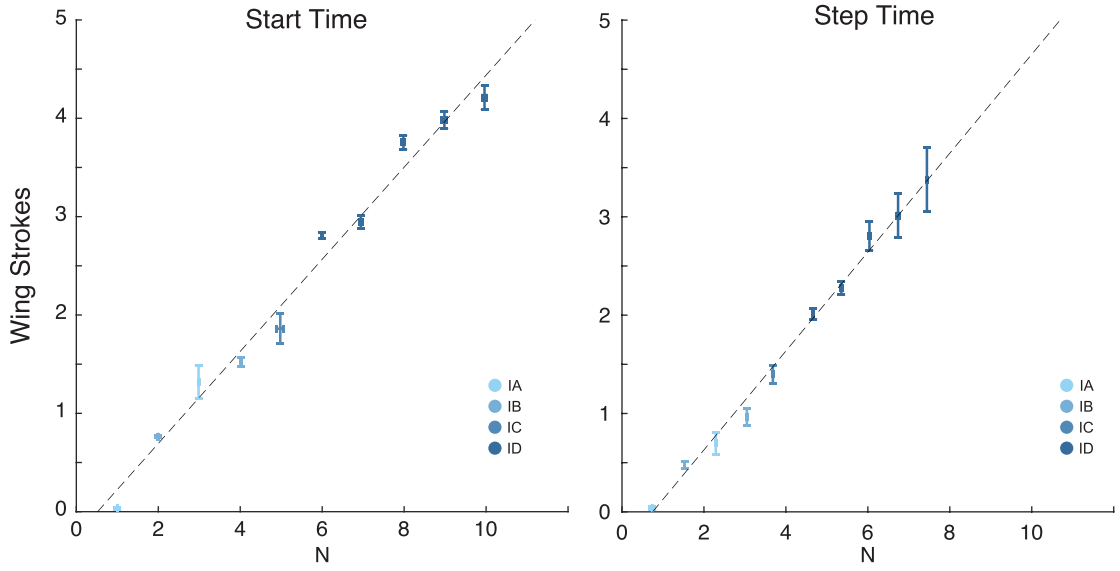

Figure B1. Start and Step Time data plotted with error bars representing standard deviation in measured N (horizontal) and t_{95} (vertical).

ORCID iDs

James Lynch https://orcid.org/0000-0003-0082-2322
Ethan S Wold https://orcid.org/0000-0002-9966-7715
Jeff Gau https://orcid.org/0000-0003-1367-3848
Simon Sponberg https://orcid.org/0000-0003-4942-4894
Nick Gravish https://orcid.org/0000-0002-9391-2476

References

[1] Josephson R K 2000 Asynchronous muscle: a primer *J. Exp.* **2722** 2713–22
[2] Weis-Fogh T 1960 A rubber-like protein in insect cuticle *J. Exp. Biol.* **37** 889–907
[3] Weis-Fogh T 1973 Quick estimates of flight fitness in hovering animals, including novel mechanisms for lift production *J. Exp. Biol.* **59** 169–230
[4] Dickinson M H and Lighton J R 1995 Muscle efficiency and elastic storage in the flight motor of drosophila *Science* **268** 87–90
[5] Lynch J, Gau J, Sponberg S and Gravish N 2021 Dimensional analysis of spring-wing systems reveals performance metrics for resonant flapping-wing flight *J. R. Soc. Interface* **18** 20200888
[6] Sane S P 2003 The aerodynamics of insect flight *J. Exp. Biol.* **206** 4191–208
[7] Ellington C P 1999 The novel aerodynamics of insect flight: applications to micro-air vehicles *J. Exp. Biol.* **202** 3439–48
[8] Jafferis N T, Graule M A and Wood R J 2016 Non-linear resonance modeling and system design improvements for underactuated flapping-wing vehicles *2016 IEEE Int. Conf. on Robotics and Automation (ICRA)* (ieeexplore.ieee.org) pp 3234–41
[9] Gau J, Wold E S, Lynch J, Gravish N and Sponberg S 2022 The hawkmoth wingbeat is not at resonance *Biol. Lett.* **18** 20220063
[10] Wold E S, Liu E, Lynch J, Gravish N and Sponberg S 2024 The Weis-Fogh number describes resonant performance tradeoffs in flapping insects *Integr. Comp. Biol.* **64** 632–643
[11] Pons A and Beatus T 2022 Distinct forms of resonant optimality within insect indirect flight motors *J. R. Soc. Interface* **19** 20220080
[12] Baek S S, Ma K Y and Fearing R S 2009 Efficient resonant drive of flapping-wing robots *2009 IEEE/RSJ Int. Conf. on Intelligent Robots and Systems* pp 2854–60
[13] Ma K Y, Chirarattananon P and Wood R J 2015 Design and fabrication of an insect-scale flying robot for control autonomy *2015 IEEE/RSJ Int. Conf. on Intelligent Robots and Systems (IROS)* (Ieeexplore.ieee.org) pp 1558–64
[14] Tu Z, Fei F, Zhang J and Deng X 2020 An at-scale tailless flapping-wing hummingbird robot. I. Design, optimization and experimental validation *IEEE Trans. Robot.* **36** 1511–25
[15] Chen Y, Zhao H, Mao J, Chirarattananon P, Helbling E F, Hyun N-seung P, Clarke D R and Wood R J 2019 Controlled flight of a microrobot powered by soft artificial muscles *Nature* **575** 324–9
[16] Mazharmanesh S, Stallard J, Medina A, Fisher A, Ando N, Tian F-B, Young J and Ravi S 2021 Performance of passively pitching flapping wings in the presence of vertical inflows *Bioinspir. Biomim.* **16** 056003
[17] Ishihara D and Horie T 2016 Passive mechanism of pitch recoil in flapping insect wings *Bioinspir. Biomim.* **12** 016008
[18] Chin D D and Lentink D 2016 Flapping wing aerodynamics: from insects to vertebrates *J. Exp. Biol.* **219** 920–32
[19] Gau J, Gemilere R, LDS-VIP FM subteam, Lynch J, Gravish N and Sponberg S 2021 Rapid frequency modulation in a resonant system: aerial perturbation recovery in hawkmoths *Proc. Biol. Sci.* **288** 20210352
[20] McGill R, Hyun N-S P and Wood R J 2022 Frequency-modulated control for insect-scale flapping-wing vehicles *IEEE Robotics and Automation Letters* pp 1–8
[21] Ellington C P 1984 The aerodynamics of hovering insect flight. I. The quasi-steady analysis *Philos. Trans. R. Soc.* B **305** 1–15
[22] Beards C 1995 *Engineering Vibration Analysis With Application to Control Systems* (Butterworth-Heinemann)
[23] Gau J, Gravish N and Sponberg S 2019 Indirect actuation reduces flight power requirements in Manduca sexta

via elastic energy exchange *J. R. Soc. Interface* **16** 20190543
[24] Whitney J P and Wood R J 2012 Conceptual design of flapping-wing micro air vehicles *Bioinspir. Biomim.* **7** 036001
[25] Dickinson M H, Lehmann F O and Sane S P 1999 Wing rotation and the aerodynamic basis of insect flight *Science* **284** 1954–60
[26] Bayiz Y E and Cheng B 2021 State-space aerodynamic model reveals high force control authority and predictability in flapping flight *J. R. Soc. Interface* **18** 20210222
[27] Deora T, Gundiah N and Sane S P 2017 Mechanics of the thorax in flies *J. Exp. Biol.* **220** 1382–95
[28] Pons A and Beatus T 2022 Elastic-bound conditions for energetically optimal elasticity and their implications for biomimetic propulsion systems *Nonlinear Dyn.* **108** 2045–74
[29] Farisenkov S E, Kolomenskiy D, Petrov P N, Engels T, Lapina N A, Lehmann F-O, Onishi R, Liu H and Polilov A A 2022 Novel flight style and light wings boost flight performance of tiny beetles *Nature* **602** 96–100
[30] Ma K Y, Chirarattananon P, Fuller S B and Wood R J 2013 Controlled flight of a biologically inspired, insect-scale robot *Science* **340** 603–7
[31] Harvey C, Baliga V B, Wong J C M, Altshuler D L and Inman D J 2022 Birds can transition between stable and unstable states via wing morphing *Nature* **603** 648–53
[32] Gau J, Lynch J, Aiello B, Wold E, Gravish N and Sponberg S 2023 Bridging two insect flight modes in evolution, physiology and robophysics *Nature* **622** 767–74
[33] Reid H E, Schwab R K, Maxcer M, Peterson R K D, Johnson E L and Jankauski M 2019 Wing flexibility reduces the energetic requirements of insect flight *Bioinspir. Biomim.* **14** 056007
[34] Ellington C P 1984 The aerodynamics of hovering insect flight. IV. Aerodynamic mechanisms *Philos. Trans. R. Soc.* B **305** 79–113